JPMTR 119 | 1814
DOI 10.14622/JPMTR-1814
UDC 655|004.08-024.72

Review paper
Received: 2018-07-09
Accepted: 2019-01-04

Printing of low-cost chipless RFID tags

Sika Shrestha, Ramprakash Yerramilli and Nemai Chandra Karmakar

Department of Electrical and Computer System Engineering,
Monash University, Australia

sika.shrestha@monash.edu
ramprakash.yerramilli@monash.edu
nemai.karmakar@monash.edu

Abstract

Chipless radio frequency identification (RFID) is a highly attractive and easy-to-operate technology allowing automated scanning of goods without any human intervention. It is a low-cost alternative to chip-based technology with few constraints. The flexibility to use low-cost printing techniques makes the chipless tags cost-effective to be useful as a competitive technology. In this paper, we review and compare the most common printing techniques for fabricating chipless RFID tags. Some of the issues encountered during printing of tags were identified and solutions to achieve better outcome were suggested. Most importantly, the advantages and limitations of the printing techniques were highlighted from a perspective of a vast amount of work done by various research teams worldwide. The review is an attempt to cover the basic aspects of conductive ink printing to fabricate functional chipless RFID tags. It is intended to guide researchers in tag printing using common printing techniques.

Keywords: inkjet printing, screen printing, flexographic printing, gravure printing, automatic identification and data capture technology

1. Introduction

Automatic identification and data capture (AIDC) technologies have been used to identify objects, collect the data and send the data into a computer system for further processing. The convergence of AIDC and network technologies is a predominant section of the Internet of things (IoT). The AIDC technology can collect and retrieve the data at every point of transaction and its integration with network entities can distribute the information for various applications in IoT. We can find several types of AIDC technologies such as barcodes, magnetic strips, smart cards, optical character recognition (OCR) and radio frequency identification (RFID). Barcode technology has become ubiquitous due to their high information density, low cost and direct printability over the items. The technology is considered as laborious as each item has to be scanned individually at the line of sight.

On the other hand, conventional RFID technology uses radio waves and can identify items held inside a case or hidden behind items in a shelf. It does not require line-of-sight communication with the tagged object and therefore requires minimal human participation between the data carrying device which, in most cases, is a transponder (tag) and a separate interrogator (detector). The detector can count multiple objects quickly and identify them simultaneously. For these reasons, the technology has emerged as the most efficient wireless transmission and reception technique for data capture, authentication and automatic identification. However, the penetration of conventional RFID technology into the supply-chain market is limited by the cost associated mainly with the silicon (Si) chip. This can be easily understood from Figure 1, where the basic steps involved in the fabrication of a conventional RFID tag are shown.

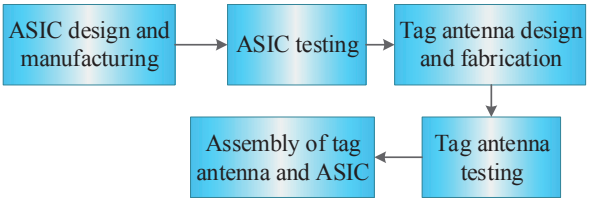

Figure 1: Steps in RFID tag fabrication, adopted from Preradovic (2009)

The fabrication process starts with the design and manufacturing of application-specific integrated circuit (ASIC). This integrated circuit (IC) is one of the

most important components in a conventional RFID tag detection system and contains the memory and tag data. The IC fabrication process generally includes a series of photolithographic and chemical processing steps such as photoresist deposition, removal, patterning, and tuning of the electrical properties (Shao, 2014).

Silicon chip based tags owe their high cost to its selection, processing, and assembly with other components such as batteries and antennas (Violino, 2004; Anee and Karmakar, 2012). Along with the advancement of wafer processing technology and consequent reduction in Si price, the size of an IC chip also shrunk making it more attractive for RFID applications. The discussion about the 5-cent RFID tag (Violino, 2004; Anee and Karmakar, 2012) concluded that advancement in IC chip technology will not be able to reduce the tag price below 5 cents to make it cost-effective for mass deployment for various reasons.

Chipless RFID technology is attractive for low-cost applications over Si-chip based tags due to the absence of the steps shown in Figure 1. The building blocks of a chipless RFID system are shown in Figure 2. The main function of a tag is to generate an identification code. The data encoding can be based on time, frequency and phase domain. Coding can also be done using hybrid domain and radar imaging. Since chipless tag does not have data processing capability, signal processing is entirely done in the reader electronics. A chipless tag reader, therefore, has a new set of design requirements and challenges compared to a chip-based tag reader.

A fully functional chipless tag reader requires an RF transceiver and a digital board with overall system integration. The reader interrogates the tag with an ultra-wide band (UWB) radiation envelope of constant amplitude. The tag returns a backscattering signal in the form of data stream known as the identification data (ID). A reader captures and processes the data to recognize and trace the tag ID. The middleware performs the signal processing for the detection of tag ID from the received signals with error correction and anti-collision algorithms (Anee and Karmakar, 2012).

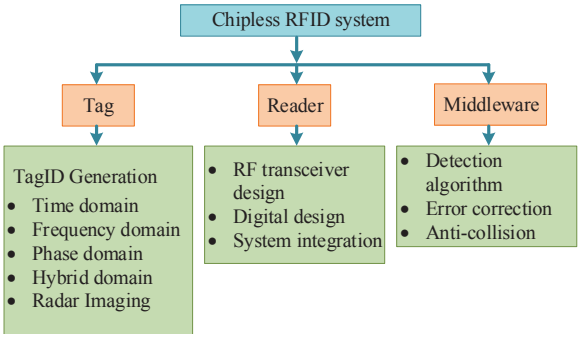

Figure 2: Basics of a chipless RFID system

Printing of chipless tags using common printing processes is considered as an option to reduce the price of tags below a cent mark (Haak, 2018). Walmart deployed electronic article surveillance (EAS) 1-bit tags based on Si-chip technology in retail market. Walmart's requirement amounts to several million of tags per year. At a tag price of 5 to 10 cents, the cost for supply of several million tags for a retail application would not be cost-effective (Kosasi, Kom and Saragih, 2014; Vowels, 2006; Jewell, et al., 2015). To be cost-effective, the sale of low-priced goods at low-profit margins would require the tag price to be ≤ 1 cent. It has been predicted that 700 billion chipless tags will be sold in 2019, if the tag price falls below a cent. Market report from TechNavio (2017) mentioned that global chipless RFID market will grow at a compound annual growth rate (CAGR) of 27.43 % during the period 2017–2021. Inventory management involving tracking of products, assets, stored components and finished products has become an imperative asset of many companies and hence the demand for the supply of low-cost tags is in surge. The chance of counterfeiting of a polymer banknote issued by Reserve Bank of Australia and by governments in other countries, is an accepted threat to the banknote business incurring financial losses (Cowling, 2011). The printing of chipless tags is considered as an attractive proposition for banknote protection, if manufactured in large volumes, at a price of ≤ 1 cent per tag. Justification for the price of the tag is linked to the low-cost materials used in any printing industry compared to fabrication of tags using printed circuit boards (PCB) technology.

Research papers covering various aspects of chipless tag design (Huang and Su, 2017; Martinez and van der Weide, 2016; Noor, et al., 2016; Preradovic and Menicanin, 2016; Rance, et al., 2016), reader development (Karmakar, et al., 2013; Preradovic and Karmakar, 2010; Koswatta and Karmakar, 2012) and tag ID detection (Kalansuriya, et al., 2012; Kalansuriya and Karmakar, 2012; Anee and Karmakar, 2012) were sighted. The reading of tag identification data depends on the detectability of tag radar cross-section (RCS) response over the frequency range. In real-world scenario, the cluttering signals, the leakage of environmental reflections from the transmitter and the interference from surrounding tags attenuate the RCS response. It is, therefore, vitally important to look for improved signal detection electronics.

In this paper, we reviewed common tag printing techniques such as inkjet, screen, flexographic and gravure printing processes using conductive silver ink. Inkjet printing is a direct technique allowing printing of tags on any type of substrate. Screen printing is a well-established laboratory and industrial technique, while gravure and flexography are well-known high speed printing techniques for high volume production

of tags. We cover the basics of the printing processes (Section 2), tag performance comparison reported in the literature (Section 3), tag performance study vs printing parameters (Section 4) and conclusions from this work (Section 5) in the rest of the review article.

2. Printing of chipless tags

The printing of chipless tags takes place through the deposition of conductive ink stripes on a substrate using a suitable design by any of the printing techniques mentioned above. The printed tags are sintered at suitable temperature to increase the electrical conductivity of the tracks. A schematic of the printing and sintering process is shown in Figure 3.

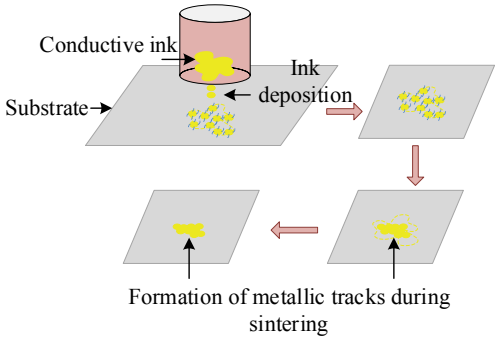

Figure 3: Printing of conductive ink tracks by direct ink deposition and subsequent sintering, adopted from Shao (2014)

2.1 Inkjet printing

The versatility of inkjet printing as a digital and non-impact printing process allows it to print directly from computer data onto virtually any substrate size. Inkjet printing requires very complex ink formulation. These formulations may be water or solvent-based. A few varieties of formulations might need to undergo hot-melt or UV-curing steps. The ink viscosities are around 0.01 Pa·s (Titkov, et al., 2015). The inkjet printing process is of two types: continuous inkjet and drop-on-demand (DoD). In the continuous ink jet process, the droplet generator is made of a reservoir storing ink under pressure which gets released when the generator is subjected to a vibration. The vibration increases the pressure inside the reservoir enabling a stream of fine droplets to eject from the nozzle. The droplets pass through a charged electrode and can be deflected in two different directions by means of two mutually perpendicular electric fields. The droplets which are not to be printed are deflected into a gutter and recycled while those going through the electric field, join to form a single printed line. The resolution is limited to only 60 lines per centimetre (Blayo and Pineaux, 2005), which is rather low for printed electronics.

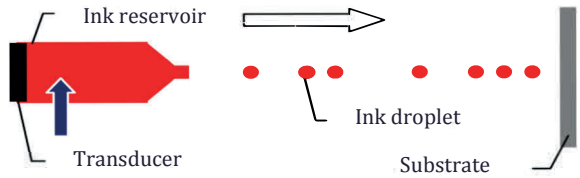

Figure 4: The inkjet drop-on-demand process

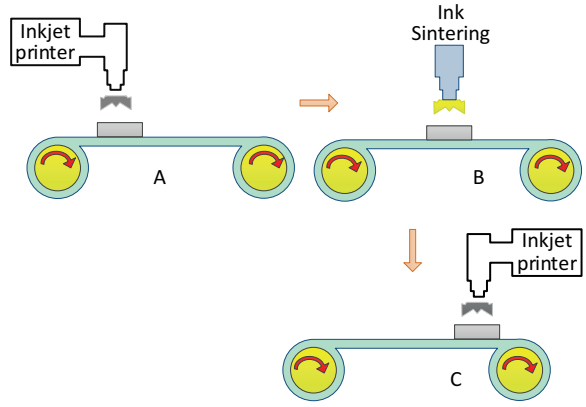

Figure 5: Inkjet printing process showing: in step (A) ink droplet hitting the substrate at the beginning of the process, in step (B) sintering of the ink droplets after they hit the surface, and in step (C) second pass of inkjet printing (multi-layer printing), adopted from Shao (2014)

In the DoD process (Figure 4), ink droplets coming out from the nozzle in the printer cartridge, sinter soon after hitting the substrate. The size of DoD droplets will be around 5 picolitres and much less at the time when they are ejected, but spreads into a diameter of 21 µm, soon after touching the substrate. Continuous lines of width of 21 µm will form after the individual droplets join together. It is common to have placement errors due to undesirable "satellite" droplets reaching specific substrate areas that should not get printed. The standard placement errors with state-of-the-art inkjet printers is approximately 10 µm at a distance of 1 mm from the print head (Cummins and Desmulliez, 2012). Edge effects are also possible, especially with thermal inkjet printers. This happens when the pressure in the reservoir increases, either due to the vibration of a piezo-element in the piezo-system or due to the blocking of the nozzle by dried ink bubbles formed due to the rapid evaporation of the solvent in the ink by the heating system.

Inkjet printing is economical in terms of ink usage as mostly, the required amount of ink is always printed. The design file is printed directly over the substrate by a print head containing conductive nanoparticle ink. Multilayer printing to build required thickness is accomplished by simply depositing a new layer on top of a cured layer (Figure 5C). Curing of ink takes place

by means of a substrate heater. A common issue in inkjet printing is clogged ink cartridges and this often requires flushing and cleaning of the cartridges to remove blockage.

2.2 Screen printing

In flat-bed screen printing, the ink is transferred to the substrate through a stencil containing the tag pattern. The stencil made of fabric is stretched on a frame to enable pressure to be applied to it by a squeegee (Figure 6). Conductive ink is deposited over the stencil by a spatula in an empty area below the design. In the next step, the ink is drawn across the tag pattern by the squeegee forcing it to go through the stencil. In the rotary screen printing process, the stencil will be cylindrical in shape. The ink is poured inside the cylinder and is forced by the squeegee also located within the cylinder, to get released to the substrate, during cylinder rotations.

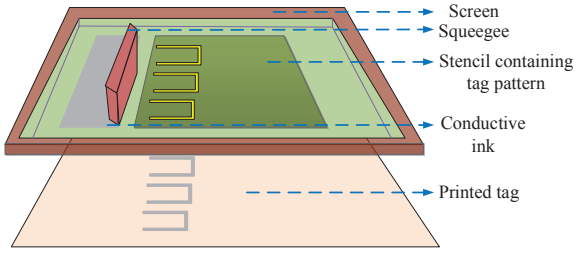

Figure 6: Screen printing of RFID tags

As a first step of the manual screen printing process, the frame will be held in a position above the substrate. In the second step, the ink is dragged along the screen by a squeegee using gentle hand pressure enabling it to flood the mesh openings. This is easily done by moving the squeegee upwards from the bottom of the screen at 45° angle. In the third step, the frame is set to sit exactly over the substrate. In this step, it will be necessary to flip the squeegee horizontally, collect the ink at one place, and get ready to drag it along the stencil and push downwards for printing to happen. In the fourth and final step, the ink is dragged along the stencil in a downward direction, beginning at the location where the squeegee was halted in the previous step (top of the screen), by applying increased hand pressure. This ensures release of the ink held in the mesh pores to the substrate placed beneath the screen.

The various parts of screen-printer and the overall printing process is shown in Figure 6. The mesh size, emulsion thickness, applied squeegee pressure and ink viscosity are optimized to obtain printing uniformity and reproducibility between runs. Screen-printing inks have viscosities in the range of 0.1 Pa·s to 10 Pa·s (Jewell, et al., 2015). It is possible to print thin to moderately thicker films, typically from 20 µm to 50 µm (Merilampi, et al., 2010) in thickness using the viscous inks. Due to the flexibility to print variable thickness, screen printing has been in practice for micro-electronic printing. Drying of inks usually occurs through a thermal process whereby the solvent in the ink is evaporated by hot air blowers, IR heaters or radiant heat from UV lamps.

The screen-printing process has its limitations of resolution and speed. The maximum printable resolution remains usually at 30 lines per cm and print speed is limited to 12 m/min. In comparison, gravure and flexographic printing processes are fast with maximum print speeds exceeding 200 m/min. The print speed has a direct effect on the conductive film resistance. Increasing the print speed from 3 m/min to 12 m/min increases the resistance by 8 %. The uniformity and print tolerance are influenced by the print speed. An improvement of 21 % was observed in print uniformity by changing the speed from 3 m/min to 9 m/min. The printing tolerance was found to reach a fixed value of 10 % (Salam, et al., 2011) for print speeds ≥ 120 m/min. In laboratory phase trials, where a specific design needs to be printed to verify proof-of-concept, a print speed of 20 m/min is sufficient in any flexographic or gravure process.

2.3 Flexography printing

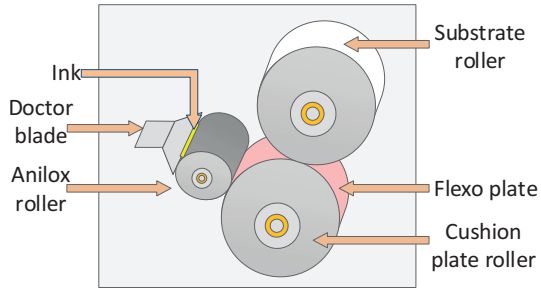

Figure 7: Flexography printing process printing process for chipless RFID tag

The basic process and the various parts of a flexographic printer are shown in Figure 7. The operating principle is described below.

The process allows printing on smooth and rough surfaces of plastic films and paper substrates, by a proper selection of a combination of resilient plates and low viscosity inks. The flexographic process consists of four components, namely (1) flexo plate, (2) anilox roller, (3) flexo plate cylinder, and (4) substrate roller. The flexographic image carrier uses a raised image attached to a cylinder. The flexo plate cylinder, covered with flexo plate made up of rubber, picks up ink from an anilox roller and delivers a smooth flow of ink to the substrate roller. The anilox roller surface contains mil-

lions of cells to hold and carry fixed volumes of ink to the plate, during a print run. The number of cells vary from 80 to 1200 per inch. Ink is delivered to the plate in a controlled manner from the anilox roller and any excess ink is wiped off by a doctor blade (Figure 7). In this way, a thin layer of ink is transferred to the flexo plate, and then to the substrate backed by a substrate roller. The pressure between the anilox roller and the plate, and that between the plate and the substrate is mechanically controlled.

The inks used in Flexography printing can be solvent or water-based. Solvent-based inks dry fast under the application of heat by thermal heat blowers or by using an IR lamp heater. Ultraviolet curable inks can also be used. Printing can take place on absorbent and non-absorbent substrates. Standard flexographic presses can accommodate a wide range of cylinder repeat lengths to match customer requirements of print length.

Flexography process for microelectronic application was tested on indium tin oxide (ITO) coated polyethylene terephthalate (PET) films (Deganello, et al., 2012) and paper substrates (Kattumenu, 2008). Deganello and co-workers were able to print lines of 0.76 µm in thickness and 75 µm in width having a sheet resistance of 1.26 Ω/sq. Another research group studied flexography printing of silver inks on different types of paper substrates (Kattumenu, et al., 2009). A minimum sheet resistivity as low as 0.35 Ω/sq at 2 µm ink film thickness was reported.

Flexographic printing on low temperature co-fired ceramic (LTCC) substrates was tested by printing a mass fraction of 30 % of silver ink using roll-to-roll (R2R) print runs in 3 to 5 passes (Faddoul, et al., 2012). The printed lines on LTCC were sintered at 850 °C for 10 min under ambient air. They showed a resistivity of 2.8×10^{-6} Ω·cm close to bulk silver resistivity and were 190 µm in width and 1.5 µm in thickness.

2.4 Gravure printing

Gravure printing is an established process for the manufacturing of high-quality images and is cost-effective. Best examples of some commercial products are wrapping paper, high-quality publications and Australian polymer banknote. Australian Research Council (ARC) funded two key R&D projects in 2009 and 2013 to develop multibit chipless RFID tags by gravure printing (Anee, et al., 2012) in collaboration with CCL Secure (formerly Securency International Pty Ltd.).

In gravure printing process (Figure 8), a large steel cylinder is electroplated with copper and engraved (or etched) to form microscopic cells on the cylinder surface by electromechanical means or laser engraving. The engraved cylinder is electroplated with chrome to reduce its wear during production runs. Low-viscosity conductive printing ink is held in a tank beneath the rotating gravure cylinder. A roll of plastic film or paper travels between the grooved cylinder and an impression cylinder. A doctor blade is used to wipe off excess ink from the cylinder during printing runs. Printing takes place on the substrate when the ink is transferred by capillary action from the cells (or grooves) to the substrate. In this way an image of the tag design (on the cylinder) gets printed on the substrate. Gravure has the capability to print a continuous image, allowing it to be a versatile printing process.

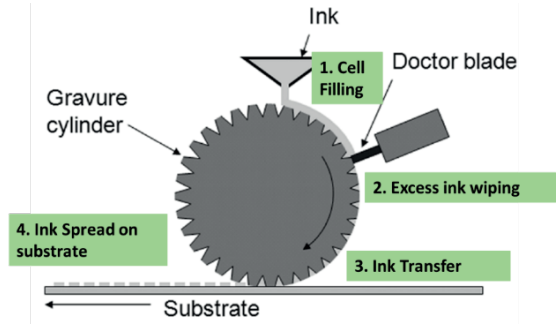

Figure 8: Different stages of gravure printing process (Sung, de la Fuente Vornbrock and Subramanian, 2010)

Gravure print quality is affected by substrate properties, ink characteristics and printer settings. Substrate properties include surface roughness of the plastic or paper, compressibility of the substrate between cylinders, porosity in the case of paper substrate, ink receptivity and wettability. Ink properties include ink chemistry, viscosity, solvent evaporation rate, drying temperature and time. Key printer setting parameters to achieve high print quality, are doctor blade angle and applied pressure, impression pressure, printing speed and flatness of the gravure cylinder across its diameter. The print quality is also affected by parameters such as, printing pressure, line width, printing direction and printing angle (Hrehorova, 2007).

Generally, gravure printing requires inks low in viscosity containing solvents that can evaporate quickly on the press during print runs. The press is generally fitted with heaters that blow hot air on the moving substrate. Low-viscosity inks are preferred over high-viscosity inks to obtain the best print quality. The shear rate was measured (Hrehorova, 2007) for water-based, solvent-based and UV-curable conductive inks. Typical viscosities of gravure conductive inks range from 0.05 Pa·s to 0.2 Pa·s (Hrehorova, et al., 2011). Inks containing a mass fraction of 75 % of silver can pose issues during printing. Kim and Sung (2015) examined the effect of using inks containing a mass fraction of 77 % of silver, having viscosity of 4 Pa·s, silver particle size between 1.4 µm and 1.5 µm and density of 3.25 g/cm^3.

The researchers found that the printability decreased gradually with decrease in line width and the trend was predominant among the tilted lines. Increasing the tilt resulted in reduced printability for the fine line patterns. The electrical resistance of the lines was found to depend on the line width and print direction. As an example, the measured resistance of a line, 25 μm in width, at normal plane with no tilting, was found to be 35.5 Ω, across 1 mm length, compared to 190 Ω measured for a line of 10 μm in width of the same length.

Pudas, et al. (2005) research group chose gravure offset printing for printing conductive inks. They added an intermediate, compressible cylinder that is inked during its contact with the grooved cylinder and, subsequently, printing takes place on the flexible substrate. By using this approach, Pudas, et al. were able to print films in the thickness range from 8 μm to 12 μm. The effect of impression pressure was tested among the gravure configurations (Clark, 2010) while attempting to print lines of 40 μm in width. Direct printing without an intermediate offset cylinder produced the best fidelity of line width. Clark observed a line widening by 55 % for direct gravure and 145 % for offset gravure printing. Ink viscosity and print direction were also shown to influence line fidelity. The combination of higher ink viscosity and high impression pressure enabled printing of a line 50.7 ± 4 μm in width against a nominated line width of 30 μm. Lines printed parallel to the print direction showed better line fidelity than those printed perpendicular to the print direction.

3. Comparison of tag features

Features of tags printed by inkjet, screen, flexographic and gravure printing processes are collected from literature and compared as shown in Appendix A.

3.1 Printing comparison

3.1.1 Inkjet printing

Inkjet printers were found to print lines with electrical conductivity comparable to tracks printed by other techniques due to the provision of overprinting capability. A 10-bit split ring resonator based tag was fabricated by inkjet printing (Herrojo, et al., 2017a) with all bits set to "1" to indicate the presence of functional resonators.

A humidity sensor based on a chipless RFID tag was fabricated and tested (Borgese, et al., 2017). The tags which were classified as frequency-selective surface (FSS) resonators, were printed by a piezoelectric printer using conductive ink on a cardboard backed by a metallic ground plane without the need for sintering. A research group (Quddious, et al., 2016) fabricated a fully passive sensor operating in the 4–5 GHz band with capability to sense either humidity or gas through changes in conductivity. The integrated sensor electrode antenna is a combination of a loop and a dipole, and enabled wireless sensing using the frequency domain chipless RFID technique. The outer-dipole arm of the antenna was used for chipless identification in the 2–3 GHz band.

A research group of Khan, et al. (2015) reported the highest code density of 3.56 bits/cm^2 (28.5 bits) for a two-layer chipless RFID tag printed on Teslin paper using a Dimatix inkjet printer and silver nanoparticle ink (UT Dots). Tags were printed on one layer and the ground plane was printed on the other layer. By printing five single layers, each of 500 nm in thickness, over one another, they were able to form a thick layer, 2.5 μm in total thickness sufficient to eliminate any skin depth (1.6 μm) related effects which are mostly observed only at low frequencies and lower conductivities. The measured conductivity of the sintered tags was found to be 6.3×10^6 S/m. The tags had shown high values of quality factor (Q) > 100.

Vena, et al. (2013a) fabricated "near-transparent" chipless 3-bit RFID scatterer tags by using strip widths of 4 mm, 3 mm, and 2.5 mm, respectively, with a total of 6-bit encoding capacity. Using the flexible features available with the inkjet printer, they were able to print the chipless tag configuration in silver ink in the first step. In the second step, they were able to reconfigure the tags by printing an overlayer in organic ink with no need for further sintering. They devised a novel coding technique based on amplitude-shift keying linking it to the resistive properties of the organic ink. Another research group (Shao, et al., 2013) demonstrated the proof-of-concept for a novel "chipless RFID coplanar LC-resonator" based tag, printed on packaging paper for operation in the frequency range of 135 MHz to 330 MHz. Using a phase-position modulation (PPM) coding technique, they were able to obtain a 4.25-bit encoding capability within a compact area.

3.1.2 Screen printing

Jeon and co-researchers (Jeon, et al., 2017) screen-printed chipless RFID tags based on dipole array structures onto plain paper using conductive ink. The tags encoded 3-bits of data by using spectral signature modulation over the frequency range 2.5–4 GHz. The tag functionality was analysed in terms of tag types, number of elements, reading range, and other parameters.

Researchers from Dresden University of Technology and Institute for Print and Media Technology, Chemnitz, Germany (Betancourt, et al., 2015) demonstrated tag

reading from a distance of 1.8 m using design methodologies of square-shaped chipless RFID tags based on FSS of plastic and paper. The application of such tags in an evacuation situation, for example in an event of a citizen's security and crisis, was explored.

The same researchers (Betancourt, et al., 2016) also reported on the design, development, fabrication and verification of octagon-shaped screen-printed tags. Besides morphological characterization and ID code verification, they undertook a complete study of the bending and folding effects on the tag. In this regard, a working tag with a bent curvature radius down to 16 mm was reported.

Continuing their work, Betancourt, et al. (2017) demonstrated a new working design of tags in the frequency range of 3–10 GHz. The design was based on genetic algorithm (GA) optimization technique. The tags were screen-printed with silver ink on low-cost substrates. They were able to operate a tag with 8-bit capacity by optimizing the frequency signature of the GA-based tags. The operated tag fits a frequency-shift keying-based coding methodology.

Nair and group (Nair, et al., 2014) fabricated a 3-bit chipless RFID tag by screen printing on a PET substrate. The proposed tag structure was formed by combining three dipoles-like structures. Microwave performance measurements were conducted in the frequency band of 2–5 GHz. Good agreement between simulation and measurement was reported for reading distance up to 1 m for 3 dBm transmitted power (dBm is a decibel referenced to the power of one milliwatt).

Blecha (2014) reported on the design, simulation and measurements of 4-bit binary-coded RFID tags fabricated by screen printing on PET foil. Different geometric dimensions and tag substrates were tested to study their influence on the resonance frequency and signal attenuation. Blecha found that resonance frequencies of particular resonance circuits depended on the length of planar resonance loops. He also found that the signal attenuation extent was dependent on the quality factor.

3.1.3 Flexographic printing

Flexographic printing is well known for its capability to print at high printing speeds of approximately 600 m/min. Printed line widths in the range of 50 µm to 100 µm and ink thicknesses up to 5 µm can be deposited at ease for any tag configuration. The technique is well suited for printing of chipless RFID tags requiring electrical conductivities in the range of 10^5 S/m to 10^7 S/m and read range distance of 1–3 m (Kattumenu, 2008). The key attraction for flexographic printing is the low production cost which could be ~0.003 USD per tag, assuming the cost of silver ink to be 1500 USD per liter (2012 price) for bulk orders (Haffarzadeh and Zervos, 2012). As a R2R printing process, it makes possible to use various low-cost materials such as paper, cardboard, and polymer film.

The quality factor Q provides the link between the frequency selectivity of a resonator and the dielectric losses due to the substrate; Q should be as large as possible to maximize the coding capacity for frequency-encoded chipless tags. It is related to the losses in the dielectric, the resistance losses in the conductors arising due to low metal content in the inks, and the radiation losses, which become dominant for configurations based on multiple resonators (Kobe, et al., 2017).

Vena, et al. (2013b) using a frequency-shift coding technique tested five C-shaped resonators in the 2–8 GHz frequency range. They fabricated copper tags using a chemical etching process on a flame resistant (FR-4) fiberglass substrate and compared their performance with those printed using an inkjet catalyst on PET film.

The performance was also compared with silver tags printed by flexography on cardboard and glossy paper. The measured sheet resistance was 0.03 Ω/sq for copper tags compared to 0.67 Ω/sq for silver-based tags. The silver tags were not sintered but were only dried at ambient temperature. The R2R production technique enabled fabrication of a 19-bit chipless tag on paper substrate.

3.1.4 Gravure printing

Gravure offset printing method provides an economically viable method for large volume production of fine-line electrical conductors. Pudas, Hagberg and Leppävuori (2004), by using gravure offset printing process and Ag-filled polymer conductive ink, were able to print 150 µm and 300 µm wide lines, with measured sheet resistance of 0.03 Ω/sq and 0.02 Ω/sq, respectively, for 7–8 µm thick tracks matching conductivity requirement for fabrication of chipless tags.

In further work, Pudas, et al. (2005) printed conductive tracks, 4–7 µm in thickness, having sheet resistance ~0.05 Ω/sq, by engraving 20–60 µm deep grooves in a gravure cylinder. They found that thick layers can be printed using high impression pressure and low print speeds. Pudas research group compared the ink thickness for gravure printing and rotary screen-printing processes. They found that the screen-printing process can only print 3–9 µm thick lines. However, the yield touched 100 % for tracks > 350 µm in width. The measured sheet resistance of 0.61 Ω/sq was found to be high and unsuitable for tag fabrication. Pudas, et al. (2005) found improved results for inductors printed by gra-

vure offset process on PET films using polymer filled silver ink. These inductors showed 2–3 times higher losses ($Q > 10$) compared to reference capacitors made in copper metal. The losses were thought to be caused by rough line edges and are mainly associated with poorly conducting polymer-filled silver inks. It is difficult to completely burn out the polymer component in silver inks at sintering temperatures below 150 °C.

3.2 Sintering

Conductive inks can be sintered at different temperatures as shown by data in Column 4 of Appendix A. The product data for inks obtained from various suppliers, contain information relating to the sintering conditions for a range of substrates. The recommended temperature for thin sheets of biaxially-oriented polypropylene (BOPP), polyvinyl chloride (PVC) and paper is approximately 100 °C. For nylon and textile substrates, the safe temperature for sintering is < 70 °C. The PET and polyester films can be heated to 140–150 °C.

3.3 Tag reading, configuration, coding and signal losses

Studies on tag reading (Herrojo, et al., 2017b) based on the near-field coupling between a chain of printed and identical split-ring resonators (SRRs) acting as the tag and a reader were reported. Encoding was achieved by the presence or absence of SRRs at predefined (equidistant) positions in the chain, and tag identification was based on sequential bit reading. In a study of Jeon, et al. (2017) using a dipole array structure, the possibility of overcoming the limitations of ink conductivity to extend the read range to 2 m was reported.

In a publication by Betancourt, et al. (2015) tags were read for several rotation and tilt angles both inside and outside the anechoic chamber at a reading distance up to 1.8 m. In another publication (Vena, et al., 2013b) peak widening and overlapping of adjacent resonant modes was reported for a tag with a coding capacity of approximately 19.9 bits at a reading distance of 50 cm and 0 dBm transmitting power.

Demonstration of time domain tags based on uniform micro-strip line (UML) and linearly-tapered micro-strip line (LTML) configuration were reported (Shao, et al., 2010). The UML tags were found unreadable, but LTML tags were readable. A tag composed of three dual-rhombic loop resonators in a total size of 7 cm × 4 cm was successfully fabricated (Vena, et al., 2013a) and operated within the 3–6 GHz band.

Periodical-like structure based tags were fabricated and reported (Betancourt, et al., 2016) as an effective way to increase the read range distance to 3.5 m using a peak-based codification technique. A special printing method using a hybrid of analog and digital printing system was reported for printing of an unique antennae (Chopra, Kazmaier and Smith, 2009). The tag fabrication comprised printing of a RFID antenna pattern with disconnected wire segments as a first step, followed by a second step of printing aiming to interconnect the disconnected wire segments to the final RFID antenna.

Signal losses from a tag due to poor conductivity and methods to compensate losses, by printing large track widths of 4 mm, 3 mm and 2.5 mm were reported (Vena, et al., 2013a). The large track widths were found not feasible for designing compact-sized tags with high data bit density.

In some cases, substrate roughness can affect the tag performance (Shao, et al., 2013). These researchers were able to obtain an increase in electrical conductivity of the tracks by reducing the paper substrate roughness by overprinting.

4. Study of printing variables

Some of the key tag printing issues and available approaches to overcome them are summarized in Table 1.

Printing parameters that influence tag performance were reviewed in Anee, et al. (2012). Conductive inks (Oldenzijl, Gaitens and Dixon, 2010) can be water or solvent-based but must meet the occupational health and safety requirements. A study of the influence of ink conductivity on RF performance was reported (Islam and Karmakar, 2015) for a dual polarized chipless tag. They observed that low conductivity tracks resulted in an increase in resonant bandwidth, a decrease in the frequency depth notch and a shift in the resonant frequency.

Inks with low metal content also caused a loss of electromagnetic (EM) response. A decrease in electrical conductivity from 3×10^6 S/m to 3×10^5 S/m with a 3-dB loss in the EM response, has been reported (Vena, et al., 2013b).

The following selection criteria for conductive inks can be used as a guideline to fabricate printed RFID tags with reasonable microwave performance, according to Anee, et al. (2012):

- Electrical conductivity ≥ 10^6 S/m to 10^7 S/m
- Sheet resistance ≤ 5 mΩ/sq to 10 mΩ/sq
- Metal pigment content > 50 %
- Sintering temperature < 150 °C
- Sintering time 1 min to 30 min.

Table 1: Some common printing issues and solutions

Issue	Solution
Ink spreads into the gaps between lines for thicker tags printed by screen, flexographic and gravure printing.	Use inkjet printing technique and overprint to increase thickness.
Tags printed by screen, flexo and gravure printing processes display low electrical conductivity.	Use low resolution flexography printing process to obtain higher electrical conductivity. Increase cylinder groove depth in gravure printing. Use low count mesh in screen printing.
Resin-based inks need sintering at 140 °C to obtain high electrical conductivity from printed tracks and therefore are unsuitable for certain substrates.	Use binder-free conductive printing inks that offer flexibility to sinter at low temperatures. Alternatively, use high-power laser cutting technique for cutting tag patterns from a metal foil.
Tags printed with conductive inks with ≤ 50 % metal content display low Q factors.	Use inks with metal content ≥ 70 % to obtain high Q factors. Alternatively, consider using metal foils if cost is not an issue.
Difficulty in replication to obtain higher RCS and long reading range.	Use high metal content inks, metal foils and additive printing techniques.

The substrate dielectric permittivity and loss tangent has direct influence on the microwave performance of the printed tags. Increase in the resonant bandwidth, attenuation level and resonant frequency has been observed (Islam and Karmakar, 2015) on tags printed over substrates with low permittivity (ε_r). The loss tangent (tan δ) representing the RF signal loss was found to depend on the substrate material. Islam and Karmakar also observed attenuation of frequency notch depth from 35 dBsm at tan δ = 0.002 to 10 dBsm at tan δ = 0.1 (dBsm is a decibel value referenced to a square meter). Poor print adhesion is often the result of incorrect ink sintering conditions. As a rule, ink with low surface tension will adhere better to any substrate with high surface energy. For this reason, substrates are plasma corona discharge treated before printing and it is a standard practice throughout the printing industry.

In Appendix B we listed few solvent-based screen printing inks. In Appendix C, we summarized key ink, printing and substrate related parameters and design considerations influencing the tag performance.

5. Conclusions

Printed tags have issues with tag detection mainly because of low electrical conductivity arising from low print thickness. It is possible to fabricate chipless RFID tags on any plastic or paper substrate by screen printing conductive inks in a simple setup at reduced cost. Inkjet printing is a popular technique and offers savings on ink usage, cost of substrate heating, and has the flexibility for overprinting to build up print thickness. Gravure and flexographic printing are suited for low-cost R2R manufacturing due to their ability to print at high speeds, up to 600 m/min. The performance of printed tags showing considerable spread of RCS response is directly associated with low track conductivity. The ink market is flooded with a variety of conductive inks and pastes to suit a variety of printing techniques and intended applications. In our knowledge, conductive inks that can dry at ≤ 70 °C on press and are suitable for high-speed gravure and flexographic printing process are not commercially available. For this reason, fully printed multibit chipless RFID tags at < 1 cent price per tag cannot be realized.

References

Anee, R.-E-A. and Karmakar, N.C., 2012. Efficient collision detection method in chipless RFID systems. In: *7th International Conference on Electrical and Computer Engineering, ICECE 2012*. Dhaka, Bangladesh, 20–22 December, 2012. IEEE, pp. 830–833. https://doi.org/10.1109/ICECE.2012.6471679.

Anee, R.-E-A., Roy, S.M., Karmakar, N.C., Yerramilli, R. and Swiegers, G.F., 2012. Printing techniques and performance of chipless tag design on flexible low-cost thin-film substrates. In: N.V. Karmakar, ed. *Chipless and conventional radio frequency identification: systems for ubiquitous tagging.* Hershey, PA, USA: IGI Global. https://doi.org/10.4018/978-1-4666-1616-5.ch009.

Betancourt, D., Barahona, M., Haase, K., Schmidt, G., Hübler, A. and Elinger, F., 2017. Design of printed chipless-RFID tags with QR-code appearance based on genetic algorithm. *IEEE Transactions on Antennas and Propagation,* 65(5), pp. 2190–2195. https://doi.org/10.1109/TAP.2017.2684193.

Betancourt, D., Haase, K., Hübler, A. and Ellinger, F., 2016. Bending and folding effect study of flexible fully printed and late-stage codified octagonal chipless RFID tags. *IEEE Transactions on Antennas and Propagation,* 64(7), pp. 2815–2823. https://doi.org/10.1109/TAP.2016.2559522.

Betancourt, D., Nair, R., Haase, K., Schmidt, G., Bellmann, M., Höft, D., Hübler, A. and Ellinger, F., 2015. Square-shape fully printed chipless RFID tag and its applications in evacuation procedures. In: *9th European Conference on Antennas and Propagation (EuCAP)*. Lisbon, Portugal, 13–17 April 2015. IEEE.

Blayo, A. and Pineaux, B., 2005. Printing processes and their potential for RFID printing. In: *Proceedings of the 2005 joint conference on Smart objects and ambient inteligence: innovative context-aware services: usages and technologies*. Grenoble, France, 12–14 October 2014. New York, NY, USA: ACM, pp. 27–30. https://doi.org/10.1145/1107548.1107559.

Blecha, T., 2014. Screen printed chipless RFID tags. In: *Proceedings of the 2014 37th International Spring Seminar on Electronics Technology (ISSE)*. Dresden, Germany, 7–11 May 2014. IEEE, pp. 143–146. https://doi.org/10.1109/ISSE.2014.6887581.

Borgese, M., Dicandia, F.A., Costa, F., Genovesi, S. and Manara, G., 2017. An inkjet printed chipless RFID sensor for wireless humidity monitoring. *IEEE Sensors Journal,* 17(15), pp. 4699–4707. https://doi.org/10.1109/JSEN.2017.2712190.

Chopra, N., Kazmaier, P.M. and Smith, P.F., Xerox Corporation. 2009. Individually unique hybrid printed antennae for chipless RFID applications. E.U. Pat. EP 2 065 837 A1.

Clark, D.A., 2010. *Major trends in gravure printed electronics*. [pdf] California Polytechnic State University. Available at: <https://pdfs.semanticscholar.org/eaee/6771099cc878349abdb40f45909fc9ea1286.pdf> [Accessed June 2018].

Cowling, A., 2011. Recent trends in counterfeiting. *RBA Bulletin*, September, pp. 63–70.

Cummins, G. and Desmulliez, M.P.Y., 2012. Inkjet printing of conductive materials: a review. *Circuit world,* 38(4), pp. 193–213. https://doi.org/10.1108/03056121211280413.

Deganello, D., Cherry, J.A., Gethin, D.T. and Claypole, T.C., 2012. Impact of metered ink volume on reel-to-reel flexographic printed conductive networks for enhanced thin film conductivity. *Thin Solid Films,* 520(6), pp. 2233–2237. https://doi.org/10.1016/j.tsf.2011.08.050.

Faddoul, R., Reverdy-Bruas, N., Blayo, A., Haas, T. and Zeilmann, C., 2012. Optimisation of silver paste for flexography printing on LTCC substrate. *Microelectronics Reliability,* 52(7), pp. 1483–1491. https://doi.org/10.1016/j.microrel.2012.03.004.

Haak, D., 2018. *Will we get a one cent RFID tag?* [online] Available at: <https://www.linkedin.com/pulse/we-get-one-cent-rfid-tag-danny-haak/> [Accessed November 2018].

Haffarzadeh, K. and Zervos, H., 2012. *Conductive ink markets 2012–2018 silver & copper inks & pastes and beyond*. Boston, MA, USA: IDTechEX.

Herrojo, C., Mata-Contreras, J., Núñez, A., Paredes, F., Ramon, E. and Martín, F., 2017a. Near-field chipless-RFID system with high data capacity for security and authentication applications. *IEEE Transactions on Microwave Theory and Techniques,* 65(12), pp. 5298–5308. https://doi.org/10.1109/TMTT.2017.2768029.

Herrojo, C., Mata-Contreras, J., Paredes, F., Núñez, A., Ramon, E. and Martín, F., 2017b. Near-field chipless-RFID tags with sequential bit reading implemented in plastic substrates. *Journal of Magnetism and Magnetic Materials,* 459, pp. 322–327. https://doi.org/10.1016/j.jmmm.2017.10.005.

Hrehorova, E., 2007. *Materials and processes for printed electronics: evaluation of gravure printing in electronics manufacture*. PhD dissertation. Western Michigan University.

Hrehorova, E., Rebros, M., Pekarovicova, A., Bazuin, B., Ranganathan, A., Garner, S., Merz, G., Tosch, J. and Boudreau, R., 2011. Gravure printing of conductive inks on glass substrates for applications in printed electronics. *Journal of Display Technology*, 7(6), pp. 318–324.

Huang, H.-F. and Su, L., 2017. A compact dual-polarized chipless RFID tag by using nested concentric square loops. *IEEE Antennas and Wireless Propagation Letters,* 16, pp. 1036–1039. https://doi.org/10.1109/LAWP.2016.2618928.

Islam, M.A. and Karmakar, N.C., 2015. Real-World implementation challenges of a novel dual-polarized compact printable chipless RFID tag. *IEEE Transactions on Microwave Theory and Techniques,* 63(12), pp. 4581–4591. https://doi.org/10.1109/TMTT.2015.2495285.

Jeon, D., Kim, M.-S., Ryu, S.-J., Lee, D.-H. and Kim, J.-K., 2017. Fully printed chipless RFID tags using dipole array structures with enhanced reading ranges. *Journal of Electromagnetic Engineering And Science,* 17(3), pp. 159–164. http://dx.doi.org/10.5515/JKIEES.2017.17.3.159.

Jewell, E., Hamblyn, S., Claypole, T. and Gethin, D., 2015. Deposition of high conductivity low silver content materials by screen printing. *Coatings*, 5(2), pp. 172–185. https://doi.org/10.3390/coatings5020172.

Kalansuriya, P. and Karmakar, N., 2012. UWB-IR based detection for frequency-spectra based chipless RFID. In: *2012 IEEE/MTT_S International Microwave Symposium Digest.* Montreal, Canada, 17–22 June 2012. IEEE. http://dx.doi.org/10.1109/MWSYM.2012.6259704.

Kalansuriya, P., Karmakar, N.C. and Viterbo, E., 2012. On the detection of frequency-spectra-based chipless RFID using UWB impulsed interrogation. *IEEE Transactions on Microwave Theory and Techniques,* 60(12), pp. 4187–4197. http://dx.doi.org/10.1109/TMTT.2012.2222920.

Karmakar, N.C., Koswatta, R., Kalansuriya, P. and E-Azim, R., 2013. *Chipless RFID reader architecture.* Boston, MA, USA: Artech House.

Kattumenu, R., Rebros, M., Joyce, M., Fleming, P.D. and Neelgund, G., 2009. Effect of substrate properties on conductive traces printed with silver-based flexographic ink. *Nordic Pulp and Paper Research Journal,* 24(1), pp. 101–106. https://doi.org/10.3183/npprj-2009-24-01-p101-106.

Kattumenu, R.C., 2008. *Flexography printing of silver based conductive inks on packaging substrates*. PhD dissertation. Western Michigan Unversity.

Khan, M.M., Tahir, F.A., Farooqui, M.F., Shamim, A. and Cheema, H.M., 2015. 3.56 bits/cm^2 compact inkjet printed and application specific chipless RFID tag. *IEEE Antennas and Wireless Propagation Letters,* 15, pp. 1091–1112. https://doi.org/10.1109/LAWP.2015.2494864.

Kim, S. and Sung, H.J., 2015. Effect of printing parameters on gravure patterning with conductive silver ink. *Journal of Micromechanics and Microengineering*, 25(4): 045004. https://doi.org/10.1088/0960-1317/25/4/045004.

Kobe, O.B., Chuma, J., Jamisola Jr, R. and Chose, M. 2017. A review on quality factor enhanced on-chip microwave planar resonators. *Engineering Science and Technology*, 20(2), pp. 460–466. https://doi.org/10.1016/j.jestch.2016.09.024.

Kosasi, S., Kom, M. and Saragih, H., 2014. How RFID technology boosts Walmart's supply chain management. *International Journal of Information Technology and Business Management*, 24(1), pp. 29–37.

Koswatta, R.V. and Karmakar, N.C., 2012. A novel reader architecture based on UWB chirp signal interrogation for multiresonator-based chipless RFID tag reading. *IEEE Transactions on Microwave Theory and Techniques,* 60(9), pp. 2925–2933. https://doi.org/10.1109/TMTT.2012.2203929.

Martinez, M. and van der Weide, D., 2016. Compact single-layer depolarizing chipless RFID tag. *Microwave and Optical Technology Letters,* 58(8), pp. 1897–1900. https://doi.org/10.1002/mop.29944.

Merilampi, S.L., Bjorninen, T., Vuorimaki, A., Ukkonen, L., Ruuskanen, P. and Sydanheimo, L., 2010. The effect of conductive ink layer thickness on the functioning of printed UHF RFID antennas. *Proceedings of the IEEE,* 98(9), pp. 1610–1619. https://doi.org/10.1109/JPROC.2010.2050570.

Nair, R., Barahona, M., Betancourt, D., Schmidt, G., Bellmann, M., Höft, D., Plettemeier, D., Hubler, A. and Ellinger, F., 2014. A fully printed passive chipless RFID tag for low-cost mass production. In: *The 8th European Conference on Antennas and Propagation (EuCAP 2014)*. The Hague, Nederlands, 6–11 April 2014. IEEE, pp. 2950–2954. https://doi.org/10.1109/EuCAP.2014.6902446.

Noor, T., Habib, A., Amin, Y., Loo, J. and Tenhunen, H., 2016. High-density chipless RFID tag for temperature sensing. *Electronics Letters,* 52(8), pp. 620–622. https://doi.org/10.1049/el.2015.4488.

Oldenzijl, R., Gaitens, G. and Dixon, D., 2010. Conduct Radio Frequencies with Inks. In: C. Turcu, ed. *Radio Frequency Identification Fundamentals and Applications Design Methods and Solutions.* Rijeka, Croatia: InTech.

Preradovic, S., 2009. *Chipless RFID system for barcode replacement.* PhD thesis. Monash University.

Preradovic, S. and Karmakar, N.C., 2010. RFID readers–review and design. In: N.C. Karmakar, ed. *Handbook of smart antennas for RFID systems.* Hoboken, NJ, USA: Wiley. https://doi.org/10.1002/9780470872178.ch4.

Preradovic, S. and Menicanin, A., 2016. Printed 3-D stacked chipless RFID tag with spectral and polarization encoding capacity. In: *39th International Spring Seminar on Electronics Technology (ISSE)*. Pilsen, Czech Republic, 18–22 May 2016. IEEE, pp. 500–505. https://doi.org/10.1109/ISSE.2016.7563249.

Pudas, M., Hagberg, J. and Leppävuori, S., 2004. Gravure offset printing of polymer inks for conductors. *Progress in Organic Coatings,* 49(4), pp. 324–335. https://doi.org/10.1016/j.porgcoat.2003.09.013.

Pudas, M., Halonen, N., Granat, P. and Vähäkangas, J., 2005. Gravure printing of conductive particulate polymer inks on flexible substrates. *Progress in Organic Coatings,* 54(4), pp. 310–316. https://doi.org/10.1016/j.porgcoat.2005.07.008.

Quddious, A., Yang, S., Khan, M.M., Tahir, F.A., Shamim, A., Salama, K.N. and Cheema, H.M., 2016. Disposable, paper-based, inkjet-printed humidity and H_2S gas sensor for passive sensing applications. *Sensors,* 16(12), 2073. https://doi.org/10.3390/s16122073.

Rance, O., Siragusa, R., Lemaître-Auger, P. and Perret, E., 2016. Toward RCS magnitude level coding for chipless RFID. *IEEE Transactions on Microwave Theory and Techniques*, 64(7), pp. 2315–2325. https://doi.org/10.1109/TMTT.2016.2562625.

Salam, B., Lai, W.L., Albert, L.C.W. and Keng, L.B., 2011. Low temperature processing of copper conductive ink for printed electronics applications. In: *2011 IEEE 13th Electronics Packaging Technology Conference*. Singapore, 7–9 December 2011. IEEE, pp. 251–255. https://doi.org/10.1109/EPTC.2011.6184426.

Shao, B., 2014. *Fully printed chipless RFID tags towards item-level tracking applications.* Doctoral thesis. KTH Royal Institute of Technology.

Shao, B., Amin, Y., Chen, Q., Liu, R. and Zheng, L.-R., 2013. Directly printed packaging-paper-based chipless RFID tag with coplanar LC resonator. *IEEE Antennas and Wireless Propagation Letters,* 12, pp. 325–328. https://doi.org/10.1109/LAWP.2013.2247556.

Shao, B., Chen, Q., Amin, Y., Mendoza David, S., Liu, R. and Zheng, L.-R., 2010. An ultra-low-cost RFID tag with 1.67 Gbps data rate by ink-jet printing on paper substrate. In: *2010 IEEE Asian Solid-State Circuits Conference*. Beijing, China, 8–10 November 2010. IEEE. https://doi.org/10.1109/ASSCC.2010.5716569.

Sung, D., de la Fuente Vornbrock and Subramanian, V., 2010. Scaling and optimization of gravure-printed silver nanoparticle lines for printed electronics. *IEEE Trasactions on Components and Packaging Technologies*, 33(1), pp. 105–114. https://doi.org/10.1109/TCAPT.2009.2021464.

TechNavio, 2017. *Global chipless RFID market 2017–2021*. [online] Available at: <https://www.researchandmarkets.com/research/4r759p/global_chipless> [Accessed June 2018].

Titkov, A.I., Bukhanets, O.G., Gadirov, R.M., Yukhin, Y.M. and Lyakhov, N.Z., 2015. Conductive inks for inkjet printing based on composition of nanoparticles and organic silver salt. *Inorganic Materials: Applied Research*, 6(4), pp. 375–381.

Vena, A., Babar, A.A., Sydänheimo, L., Tentzeris, M.M. and Ukkonen, L., 2013a. A novel near-transparent ASK-reconfigurable inkjet-printed chipless RFID tag. *IEEE Antennas and Wireless Propagation Letters,* 12, pp. 753–756. https://doi.org/10.1109/LAWP.2013.2270932.

Vena, A., Perret, E., Tedjini, S., Petot Tourtollet, G. E., Delattre, A., Garet, F. and Boutant, Y., 2013b. Design of chipless RFID tags printed on paper by flexography. *IEEE Transactions on Antennas and Propagation,* 61(12), pp. 5868–5877. https://doi.org/10.1109/TAP.2013.2281742

Violino, B., 2004. The 5-cent RFID tag. *RFID Journal* [online] 1 January. Available at: <https://www.rfidjournal.com/purchase-access?type=Article&id=748&r=%2Farticles%2Fview%3F748> [Accessed June 2018].

Vowels, S.A., 2006. A strategic case for RFID: an examination of Wal-Mart and its supply-chain. In: *Proceedings of the 2006 Southern Association for Information Systems*. Jacksonville, FL, USA, 8–9 December 2006. Citeseer, pp. 148–152.

Appendix A

Comparison of chipless RFID conductive silver tag features produced by inkjet, screen, flexography and gravure printing techniques

Substrate type	Printer make	Sintering temperature (°C)	Printed Ag thickness (μm)	Sheet resistance (Ω/sq)	Conduct. (S/m)	Tag geometry	Freq. range (GHz)/ No. of bits	Literature reference
Inkjet printing								
PET	Ceradrop CeraPrinter	Room temperature dried	3.3–3.5	0.04	7.3×10^6	Split ring resonator	3–6/10	Herrojo, et al., 2017a
Paper	Brother printer	Not sintered	–	–	–	Three concentric loops	2–8/3	Borgese, et al., 2017
Photo paper	Dimatix printer	120	2	0.08	6.0×10^6	Antenna and balloon	2–3/1	Quddious, et al., 2016
Paper	Dimatix printer	120	2.5	0.06	6.3×10^6	Nested loop resonator	3–9/28.5	Khan, et al., 2015
Polyimide	Dimatix printer	150	2	0.08	6.3×10^6	Dual-rhombic loop resonator	3–6/3	(Vena, et al., 2013a)
Packaging paper (four types)	Dimatix printer	150	–	–	–	LC resonator	0.1–0.4/ 4.25	Shao, et al., 2013
Screen printing								
Plain paper	Standard screen printer	150	5–10	0.02	5.0×10^6 to 10^7	Dipole array structure	2.5–4/3	Jeon, et al., 2017
PET	Semiauto printer	120–140	4.3	0.11	2.0×10^4	Frequency domain QR like appearance	3–10/8	Betancourt, et al., 2017
135 g/m^2 paper, PET	Semiauto printer	120–140	4.4 (paper) 4.3 (PET)	0.11	2.0×10^4	Octagonal shaped tags	3–10/5	Betancourt, et al., 2017
135 g/m^2 paper, PET	Semiauto printer	120–140	4.4 (paper) 4.3 (PET)	0.11	2.0×10^4	Metallic square rings	2–5/4	Betancourt, et al., 2017
PET	Standard printer	–	–	0.08	–	Spiral resonator	1.5–2.5/4	Blecha, 2014
PET	Semiauto Printer	130	10	0.07	1.4×10^6	Dipole Structure	2–5/3	Nair, et al., 2014
Flexography printing								
Cardboard, glossy paper	Standard printer	Room temperatur	5	0.03	3.0×10^5	C-like & loop resonator	2–8/5	Vena, et al., 2013b
Gravure printing								
PET, Melinex, paper	IGT printer	70–120	10	0.05	2.0×10^5	35 mm dia inductor coil	0.915 (inductor)	Pudas, et al., 2005

Appendix B

List of conductive inks used in screen printing

Ink name	Sheet resistance	Conductivity (S/m)	Metal content (%)	Viscosity	Processing temperature
NovaCentrix [HPS-021]	2.6 mΩ/sq (at 1 mil*)	1.50×10^7	65	> 1 Pa·s	150 °C / 30 min
NovaCentrix [PSI-219]	< 40 mΩ/sq (at 3 μm DFT**)	8.33×10^6	44 ± 2	5–10 Pa·s at 10 s^{-1}	15–90 s, 140 °C, > 2 min at 80 °C
Creative Materials [118-09A]	0.019 Ω/sq/mil	2.07×10^6	85	–	80° C / 4 h; 100 °C / 1 h; 125 °C / 20 min
Advanced nano products [DGP-No]	0.01–0.05 Ω/sq/mil	–	70–80	50–150 Pa·s	120–150 °C
Ink-Tec [TEC-PA-010]	–	–	> 70	7–7.5 Pa·s	140 °C (5 min) 120–170 ˚C (2–5 min)

*mil – 0.001 inch (25.4 μm)
**DFT – Dry Film Thickness

Appendix C

List of parameters influencing the tag performance

Ink-related parameters	Ink metal content	High metal content based inks are preferable to obtain tracks with high electrical conductivity.
	Sintering condition	Low sintering temperatures are preferred for low melting point substrates. Sintering temperature can be elevated for high melting point substrates.
	Ink viscosity	Ink viscosity should be appropriate for the chosen printing technique. Viscosity is to be checked and adjusted before printing.
Printing parameters	Impression pressure (flexography, gravure and screen printing)	Impression pressure has to be adequate to obtain uniform and best printing quality. Excessive pressures may damage the substrate.
	Printing speed (flexography and gravure printing)	Has direct impact on amount of ink transfer to the substrate. Low speeds transfer more ink to the substrate, and high speeds less ink. Uniform prints are obtained at high speeds (> 60 m/min).
Substrate parameters	Dielectric permittivity	Frequency shift occurs due to difference in dielectric permittivity of substrates. The calculation of resonant frequency can be performed via equation given in Islam and Karmakar (2015).
	Loss tangent	Low values are preferred.
	Substrate height	Affects specific tag configurations that need a ground plane.
	Melting point	Higher melting point substrates are preferred for effective sintering of printed ink.
	Surface energy	Ink with lower surface tension than the substrate surface energy is preferred for best adhesion to the substrate.
Design considerations	Line width (LW) and line slot width (LS)	Printing techniques have their own limitations of printable line width: LW 60 μm / LS 20 μm for inkjet printing, LW 30 μm / LS 300 μm for gravure printing, LW 30 μm / LS 30 μm for flexography printing, and LW 60 μm / LS 60 μm for screen printing. Advisable is to ensure that electrical conductivity of the printed lines is in the optimum range for tag detection.